2015-01-1539
Published 04/14/2015

doi:10.4271/2015-01-1539
saepcmech.saejournals.org

CFD Investigation of the Effect of the Salient Flow Features in the Wake of a Generic Open-Wheel Race Car

Joshua Newbon, Robert Dominy, and David Sims-Williams
Durham University

ABSTRACT

It is well known that in motorsport the wake from an upstream vehicle can be detrimental to the handling characteristics of a following vehicle, in particular in formulae with high levels of downforce. Previous investigations have been performed to characterize the wake from an open wheel race car and its effect on a following car, either through the use of multiple vehicles or purpose-built wake generators.

This study investigates how the wake of an upstream race car impacts the aerodynamic performance of a following car in a close-following scenario. Wakes are imposed on the inlet of a CFD simulation and wake parameters (eg: velocity deficit, trailing vorticity) are directly manipulated to investigate their individual impacts on the following vehicle.

The approach provides a useful alternative to the simulation of multi-vehicle cases but a better simulation could be achieved by including wake unsteadiness from the upstream vehicle. Arguably the most significant impact of a wake on the following vehicle was found to be the rearward movement of the vehicle center of pressure. Secondary flow (eg: upwash, vorticity) on a bulk scale had the beneficial impact of moving the wake up and over the following vehicle but more localized impacts could be positive or negative according to the detailed interaction with downstream vehicle features.

CITATION: Newbon, J., Dominy, R., and Sims-Williams, D., "CFD Investigation of the Effect of the Salient Flow Features in the Wake of a Generic Open-Wheel Race Car," *SAE Int. J. Passeng. Cars - Mech. Syst.* 8(1):2015, doi:10.4271/2015-01-1539.

INTRODUCTION

The key contributor to the lap-time in the highest levels of open-wheel competition motorsport such as Indy Car and Formula 1 is high cornering velocity resulting from the very high aerodynamic downforce produced by the cars. This downforce comes with the penalty of a large and highly turbulent wake extending many car lengths downstream of the car. The wake can be used by a following vehicle to reduce aerodynamic drag aiding top speed. The wake also reduces the downforce produced by the following vehicle by upwards of 60% [1, 2, 3] and, more significantly, results in a rearward shift of the aerodynamic center of pressure resulting in increased understeer (push) and tire wear making it increasingly more difficult to follow or overtake a competitor. The recent trend to combat the lack of overtaking is the use of a drag reduction system (DRS) [4] pioneered in Formula 1 and now used in World Series by Renault and DTM (Deutsche Tourenwagen Masters) whereby the following car rear wing angle of attack is reduced in controlled locations to improve overtaking frequency.

Ground effect plays a key role in the downforce produced by Formula 1 cars, dramatically increasing their performance and leading to competition between the rule-makers and the engineers to limit car performance in the name of safety [5]. The main downforce-generating surfaces are the inverted front wing, rear wings and underfloor with rear upswept diffuser, shown in figure 1.

Figure 1. 2014 generic F1 car CAD with key downforce generating surfaces coloured green

The wake of a Formula 1 car is dominated by the counter-rotating vortex pair originating at the rear wing, which is further energized by the up wash from the rear diffuser [3, 4, 6]. Local axial velocity, stagnation and static pressure deficits are present as well as turbulence intensities in excess of 45%, figure 2. Rear wheel and diffuser corner wakes merge with the counter-rotating pair, forming the familiar mushroom shaped wake which develops before 0.5 car lengths

downstream of the rear wing. The vertical and transverse location of the vortices in the near wake is centered about the rear wing tips, meaning that pre-2009 [3, 6] the vortex pair was situated lower and further from the centerline than in current specification. Opening the DRS flap reduces downforce and thus the vortex strength, significantly reducing the secondary velocities in the wake, though turbulence intensities in excess of 20% remain on the centerline [4].

As the first aerodynamic surface to come into contact with the wake from an upstream vehicle, the front wing in ground effect has been the focus of numerous studies. The front wing contributes around 30-35% of the overall car downforce [7]. Downforce generated by an inverted wing will increase when in ground effect relative to freestream [8, 9, 10]. As the ground is approached downforce increases until a critical ride height, beyond which downforce abruptly reduces as stall occurs. As the ground clearance changes the wingtip vortex remains relatively constant in size [11, 12, 13], though core vorticity increases with reduced ride height up to peak downforce.

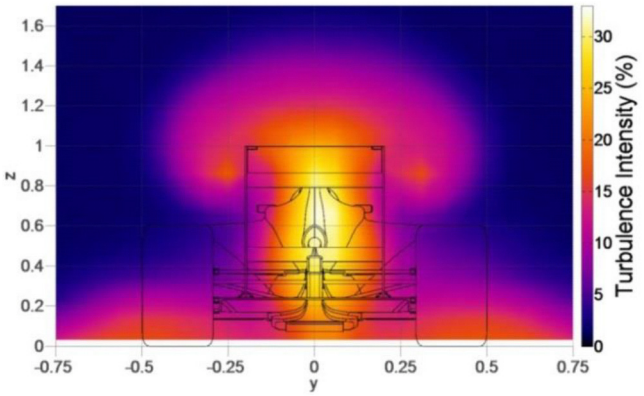

Figure 2. Turbulence intensities in wake at $0{,}5L_C$ plane downstream of a 30% scale 2011 specification Formula 1 car [4]

The effect of vehicle wakes on a wing in ground effect has been investigated using both an upstream bluff body with variable planar diffuser [14, 15, 16] and a bespoke wake generator capable of recreating the near wake of a Formula 1 car [6, 17]. The forces generated by the wing tended to decrease for all ride heights and pitch angles, with delayed stall also occurring. Delayed stall could be attributed to the high level turbulence in the wake which, depending on the transition state of the boundary layer, could also cause lower forces. Other causes could be a change in local incidence of the airflow effectively causing a change of the angle of attack. It was found that lower angle upstream diffusers created a smaller magnitude upwash which lead to higher wing lift-to-drag ratios, though these were still significantly lower than the potential freestream efficiency. For all angles of incidence more downforce was lost with the wing further out of ground effect. There is a strong horizontal component to the velocity low in the wake where the vortices are constrained by the ground. The vertical component becomes greater further out of ground effect, where any effective incidence effects occur, though as downforce is negatively affected low in the wake the horizontal onset flow must also be affecting the wing.

While isolating the front wing can be insightful, the various downforce generating surfaces are so dependent on one another that the whole system must be considered. The effect of an upstream wake on 25% Formula 1 models has been investigated [1, 3] showing a decrease in downforce of up to 35% when following $1L_C$ behind another vehicle. Aerodynamic drag is reduced by about 25% at this spacing and recovers less rapidly than downforce when a lateral offset, simulating a lane change or overtake, is introduced. When the axial separation is increased, drag is also seen to recover to the freestream value slower than downforce. Perhaps more significantly than the force loss is the rearwards shift of the center of pressure, which can move rearwards of the rear axle and was the cause of Can-Am cars overturning in the 1970s [2]. This rearward shift also results in understeer which can increase front tire wear; drivers counteracting the understeer by increasing rear wheel slip increases rear tire wear, compounding the problem.

Due to the high turbulence intensities in the wake of a Formula 1 car the effect of grid generated turbulence on wings in ground effect has been investigated [6, 18] showing delayed stall and increased downforce. Peak turbulence intensity which can be attained by grids is ~13%, which is considerably lower than the turbulence intensities found in the near wake of a race-car, figure 2, nor can it recreate on-road turbulence intensities and length scales. So active turbulence generation systems, like those found at Durham University [19, 20], FKFS [21] and Pininfarina [22], are now being favored. In the passenger vehicle sector the effect of an upstream vehicle has been investigated [23]. Like race cars the wake takes the form of a counter-rotating vortex pair, though with a centerline downwash. Aerodynamic drag of generic automobile shapes is found to reduce in the far to near wake of an upstream vehicle; lift is also sensitive to vehicle interactions. The effect of upstream turbulence generated by grids and in the CFD environment has also been investigated in the passenger vehicle sector [24, 25, 26] with less focus on forces and more on surface flow and aerodynamic unsteadiness. The turbulence results in reduced flow separation and aided pressure recovery, and unsteadiness was seen to increase which in turn increases body panel flutter.

From the beginning of 2009, the Formula 1 regulations have stipulated that the central 500mm of the front wing be a FIA-specified aerodynamically neutral section [5] to try and diminish the effect of centerline loss from the upwash of an upstream vehicle. This has not necessarily resulted in the desired increase of close racing and it has been suggested that increasing the underfloor ground effect contribution (similar to the cars of the late 1970s to early 1980s) would reduce the effect of wake interactions between vehicles; although there is no published evidence supporting this assertion.

The premise of this following study is to identify and recreate the key features of a Formula 1 car wake at the inlet of a CFD case. CFD makes it possible to manipulate different aspects of the wake directly and independently. Altering wake features independently helps to make it possible to determine their respective impacts on a following vehicle. The ultimate aim is to inform the writing of future regulations to enable closer racing.

METHODOLOGY

The vehicle geometry used for this CFD study is a generic 25% scale Formula 1 car, also used experimentally [3] in slipstreaming studies in the Durham University 2m wind tunnel. This scale is attractive experimentally as it makes it possible to accommodate multiple vehicles within the test section of a model tunnel normally used for larger scale models. The car features 2-element front and rear wings and an underfloor with upswept rear diffuser contemporary to the 2008 FIA Formula 1 regulations. The car set-up corresponds to the optimal set-up determined experimentally as described in [3].

All simulations were carried out using the EXA PowerFLOW software suite at $Re=3.1\times10^6$ based on vehicle length. PowerFLOW is a Lattice-Boltzmann based solver using a K-ε based turbulence model in the fluid with digital physics calculating wall-fluid interactions; more information of which can be found in [25, 27, 28, 29]. PowerFLOW uses a structured mesh based on variable resolution (VR) regions comprising 'voxels' (fluid cells) and 'surfels' at the junction between fluid and solid regions. The mesh used for all simulations contained 16×10^6 cells with a centerline symmetry plane split between 10 VR levels (figure 3) with a minimum voxel size of 1.5mm. Cases typically required over 1500 CPU hours and 90 GB memory running on Durham University's High Performance Computers (3600 Intel 2.4-2.66 GHz cores, 1.2 TB RAM) to reach resolution.

Figure 3. CFD domain x-y plane, VR regions 0 through 7 shown

Forces were output at 4 kHz to indicate when the simulation had converged. Vehicle drag and lift forces were shown to have reached convergence before 0.35s and time averaged measurement frames were output from 0.35 to 0.7s to remove unsteady effects.

The inlet blockage for all cases was <1% to remove wall-vehicle interactions; the walls and floor were set as velocity matched slip planes to prevent boundary layer growth. As the wheels do not feature spokes, rotating walls were used rather than a sliding mesh. The characteristic conditions for the freestream case can be seen in table 1 and were set to match standard sea level atmospheric conditions at 15°C.

Table 1. Characteristic conditions

P_∞	101325Pa
ρ	$1.225 kg/m^3$
μ	$1.18\times10^{-5} Ns/m^2$
I_X	0.01
A	$0.09375 m^2$ ($1.5 m^2$ at full scale)
L_C	1200mm (4.80m full scale)
Resolution	800 voxels/L_C

For this study a number of variable inlets are utilized to recreate various features from the wake of the generic Formula 1 car with a simulated spacing of 1 car length. To achieve this simulated separation the wake is sampled from a single-vehicle simulation and then input at the inlet of the following cases, figure 4. Previous tests have shown good correlation to a two vehicle case, more details of which can be found in [3].

As the wake develops, the vortex pair from the rear wing endplates moves inboard and upwards with the diffuser upwash (figure 19 in appendix) while increasing in size and losing momentum. The sampling plane / inlet plane was chosen to be downstream of any reversed flows, which are present in the wake up to ~$0.125L_C$ behind the car (figure 19a). So, as figure 4 shows, the wake was sampled $0.25L_C$ downstream of the car and input $0.75L_C$ upstream of the car creating the $1L_C$ separation. The domain for an external automotive CFD case would typically extend 5 to 10 car lengths upstream of the vehicle as short domains can result in non-uniform pressure or velocity fields at the inlet in order to satisfy the outlet boundary conditions. The freestream case was run for both normal and short domains and a difference of 0.08 on C_D, 0.10 on C_L and 0.5% on COP was found. Therefore, throughout results are compared with a baseline case using an equivalent "short-inlet". As the force differences investigated in this study are of significantly greater magnitude this was deemed an acceptable approach.

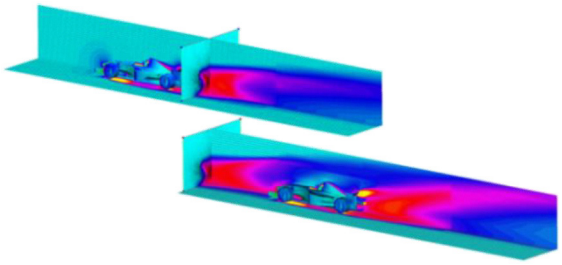

Figure 4. Wake sample and inlet planes, freestream and full input wake

In this paper the following cases are presented, shown in table 2. Firstly the freestream case, against which all the subsequent cases are compared, was run. The full wake of the 25% generic Formula 1 car was recreated at the inlet plane, which is compared to a full simulation of two vehicles. The axial velocity deficit was removed so that axial velocity equals freestream velocity and finally the sensitivity to "secondary flows" (the sum of y and z velocities $[u_Y^2+u_Z^2]^{½}$) was examined, by setting u_Y and u_Z to 0%, 90% and 110% of the full wake values.

Table 2. Summary of desired simulation outputs

Case	u_X	u_Y	u_Z	P	P_O
Full Wake	match	match	match	match	match
No axial velocity deficit	u_∞	match	match	free	match
u_Y & u_Z sensitivity	match	varied	varied	free	match

The different features of the wake are associated with different force characteristics. Axial velocity deficit is primarily a product drag resulting from the bluffness of the upstream vehicle. Secondary flows

are mostly the result of the lift or downforce generated by the wings (there will also be a small contribution to axial velocity deficit and low static pressure in the vortex cores). Reducing the magnitude of velocity deficit in the wake would therefore be associated with lower upstream vehicle drag; similarly increasing and decreasing secondary flows would result from a change of downforce. For an upstream vehicle with a given downforce level, achieving that downforce through ground effect would generally result in less secondary flow than achieving it using wings out of ground effect.

Using CFD rather than experimental methods means that changes to wake characteristics can be made directly, without engineering a family of upstream vehicles. However, the results provide a guide to the engineering direction for the design (regulation) of an upstream vehicle with a wake that has a less negative impact on a following vehicle. Assuming any future regulations will include front wing, rear wing and an upswept underfloor, the broad aerodynamic component sensitivity to the different wakes can be investigated.

In order to calculate the inlet pressure, using no secondary flows as an example, it is desired that stagnation pressure be matched to the sampled wake, figures 5 & 19. As stagnation pressure is equal to the sum of static and dynamic pressures, equation (1).

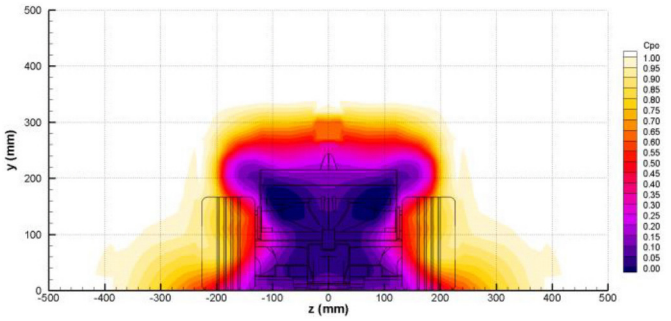

Figure 5. Sampled wake contours (stagnation pressure)

$$P_O = P + \sum q = P + \left(0.5\rho u_X^2 + 0.5\rho(u_Y^2 + u_Z^2)\right) \quad (1)$$

As the secondary flows are set to equal zero, so too are the secondary flow dynamic pressures. So if the inlet pressure were set to equal the sampled static pressure the stagnation pressure at the inlet would be too low by the sum of dynamic pressure less the y and z components, equation (2).

$$P_{INLET} + q_X \neq P + (q_X + q_{Y,Z}) \quad (2)$$

So the inlet static pressure is set as equation (3); by increasing the static pressure by the secondary dynamic pressure the stagnation pressure will be correct.

$$P_{INLET} = P + q_{Y,Z} \quad (3)$$

Using the same logic all the inlet pressures were calculated so as to match the desired outputs (table 2). Table 3 shows the inlet velocity vectors and static pressure for each case presented.

Table 3. Summary of inlet conditions for CFD cases

	Inlet Velocity			Inlet Pressure
Case	x	y	z	
Freestream	u_∞	0	0	P_∞
Full Wake	u_X	u_Y	u_Z	P
$u_X = u_\infty$	u_∞	u_Y	u_Z	$P_O - q_\infty - q_{Y,Z}$
$u_Y = u_Z = 0$	u_X	0	0	$P + q_{Y,Z}$
90% $u_{Y,Z}$	u_X	$0.9u_Y$	$0.9u_Z$	$P + 0.1q_{Y,Z}$
110% $u_{Y,Z}$	u_X	$1.1u_Y$	$1.1u_Z$	$P - 0.1q_{Y,Z}$

For all cases presented here the inlet is taken from the time-averaged output from the freestream case and so unsteady effects in the wake have been removed.

RESULTS

All the incident flow conditions are compared to a freestream case as a point of reference. The full wake created at the inlet is compared to the trailing vehicle in a two vehicle case with the same axial offset as a proof of the method presented. Finally the incident flow is modified to test vehicle sensitivities to onset flow conditions.

Freestream

In all cases the car is configured to match the highest downforce setup determined experimentally [3], which also corresponded to the greatest efficiency ($^L/_D$). Thus the car has a rake of 0.6°, nose down, with a minimum ground clearance of 9 mm at full scale to the wooden plank at the leading edge of the floor splitter. Figure 6 & 21 show the surface static pressure distribution of the car in freestream conditions. The front wing shows a suction pressure peak of $C_P = -1.4$ with the static pressure reducing toward the endplates as the flow becomes more three-dimensional. A peak suction pressure of $C_P = -1.5$ is found at the leading edge of the underfloor at the minimum ground clearance. There is then a pressure recovery over the length of the floor before another low pressure spike at the throat of the rear diffuser. The left hand bars in figure 7 show that the underfloor is the most efficient downforce-generating component on the car, with an efficiency of −14. This is almost double the front wing and six times more efficient than the rear wing. The front and rear wings each generate around 50% of the total car downforce, but the rear wing produces three times the aerodynamic drag of the front wing. The rear wing accounts for 21% of the blockage of this car, and this blockage would be significantly reduced for circuits where the penalty of drag on lap-time is higher, such as Monza. Other high drag items are the exposed front and rear wheels which contribute 37% of the car drag, the front wheels make up 35% of the frontal area and also generate lift equal to 18% of the car downforce (Figure 8).

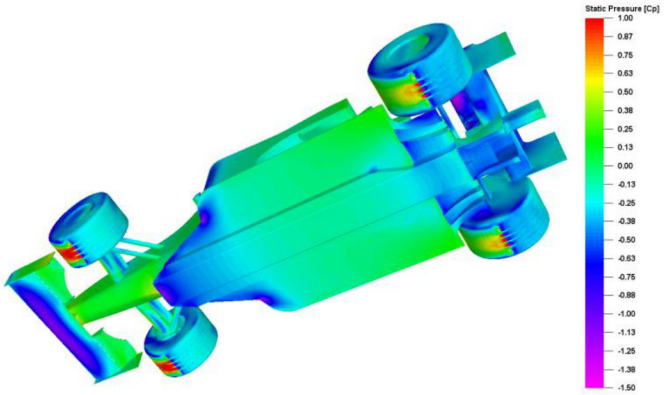

Figure 6. Freestream surface static pressure distribution

The car's upper bodywork also generates a large amount of lift, which combined with the underfloor means the car body downforce is <30% of total downforce, figure 8. The surface static pressure distribution plots in figure 6 & 18 show suctions in excess of $C_P = -0.7$ on the top and side leading edges of the sidepods and engine air intake. It should be noted that this is a generic Formula 1 geometry operating at reduced Reynolds number and it has not been optimized to the same level as a competitive vehicle.

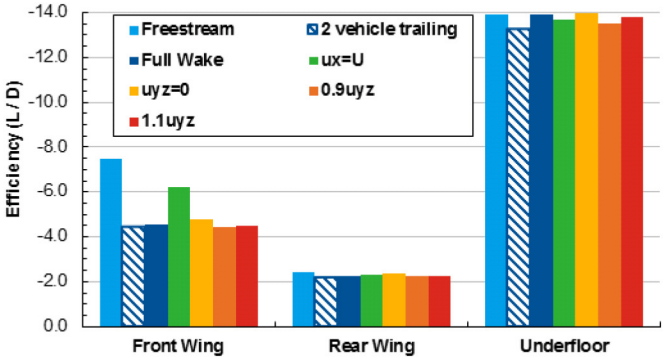

Figure 7. Individual efficiencies ($^{L}/_{D}$) of downforce generating components for different inlet conditions

Full Wake and Two Vehicles

The effect of the inlet wake on vehicle forces and efficiencies, figures 7 & 8, is very similar to running a pair of vehicles in the CFD (dark striped bar in figures 7, 8, 9 & 10), the main difference being the underfloor efficiency, which is slightly lower than results from the inlet case. There is a 3% difference in the COP location (figure 9), although the trailing vehicle COP only moves rearwards 18% (relative to the lead car) compared to 34% relative to the freestream. For both cases the combined bodywork and underfloor lift is neutral rather than downforce in the freestream case, indicating that the upper surfaces lose less lift than the underfloor loses downforce (figure 10). The center of pressure is therefore dependent on front and rear wings and wheels.

Little difference is seen between the freestream and 2 vehicle leading car component downforce and lift coefficients, light striped bar in figure 8. However small differences in the underfloor, rear wing and the front wheel lifts contibute to a 16% rearward COP compared to the freestream (figure 9). That the presence of the trailing vehicle affects the upstream vehicle is a documented phenomenon, and the differences between the full wake and trailing vehicle cases are discussed in [3] and could possibly be reduced by sampling the lead vehicle wake.

The surface pressures on the trailing car in the two vehicle case are almost identical to the inlet wake. The main pressure increase is the front wing lower surface centerline, rear wing mainplane and the underfloor. The biggest difference between the two is the suction peak at the underfloor leading edge, which is $\Delta C_P = -0.1$ compared to the inlet wake case.

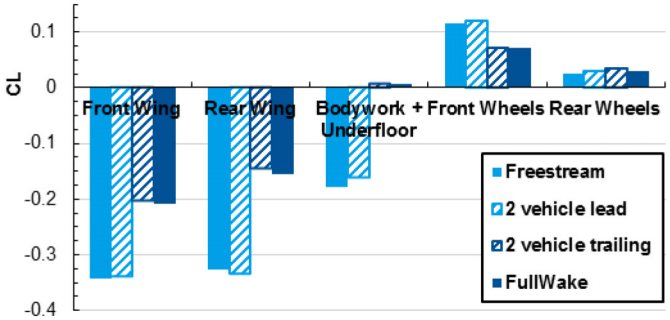

Figure 8. Component C_L based on vehicle frontal area

The key difference between the cases, from the reference of the trailing vehicle, is the simulation of unsteadiness in the wake of the lead vehicle. By running two vehicles the wake is simulated with total accuracy, while this technique currently uses a time-averaged plane to set the inlet. The wake unsteadiness also has the most significant effect on the underfloor downforce which in turn reduces the COP shift; while the front and rear wing performance and efficiency are relatively unaffected by the wake unsteadiness.

The inlet conditions for the full inlet wake (figure 22) shows very good correlation with the freestream sampled wake; especially the axial velocity and secondary flows, figures 5 & 19. The absolute magnitudes of velocity are accurately recreated, so too are the shape and locations of the contour levels. Static and stagnation pressures are less accurately recreated, with a $\Delta C_P = 0.05$ (1 contour level) difference on both. The shape of the stagnation pressure deficit is recreated despite the small difference of the pressure coefficient.

The loss of fine details in the inlet contours can be attributed to the scale of the input grid, which is less dense and uniform when compared to voxel scale. Constraining the boundary conditions over the whole inlet using a 100,000 point grid with mesh density 10mm×10mm proved more accurate than using a smaller grid concentrated about the highest deviation contours in the wake and allowing PowerFLOW to interpolate pressures and velocities over the rest of the inlet area.

The inlet wake results in a 37% rearward shift of the center of pressure, figure 9, the consequence of which would be a considerable change of the handling balance towards understeer (push). The aerodynamic efficiency of the car decreases by 60%, though the efficiency of the sprung component (i.e. all but wheels) of the car is only halved. This is due in part to a relative increase of the wheel lifts

as a percentage of the car downforce. Both the change in lift and COP are obviously very significant to the performance of the following car.

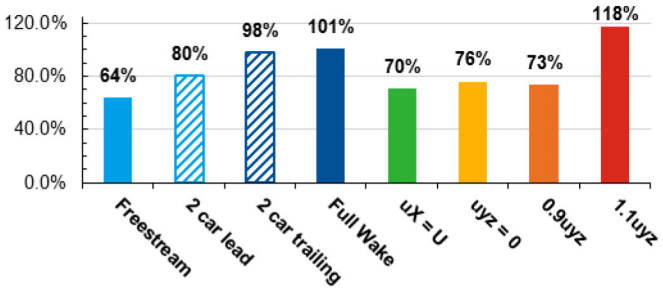

Figure 9. Percentage of downforce on rear axle (COP from front axle) for wake inlet cases

The efficiency of the front wing, figure 7, is the most impacted by the upstream wake while rear wing and underfloor $^{L}/_{D}$ remain approximately constant. Looking at drag and lift as a percentage of the freestream values though, figure 10, the front wing loses less downforce than both the underfloor and rear wings. Drag for the front wing remains consistent to the freestream case though while rear wing and underfloor drag drop at the same rate as downforce. This suggests that the rear wing and underfloor losses are related to the velocity deficit. While the front wing is subjected to secondary flow effects which result in downforce loss but not drag.

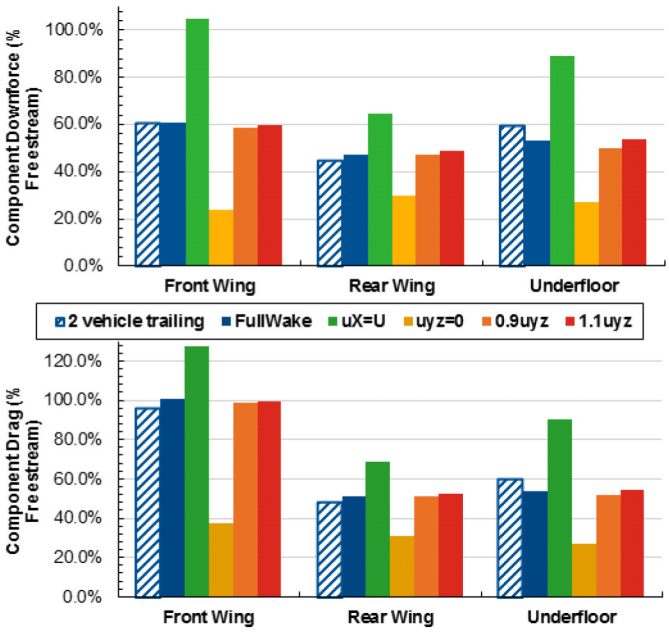

Figure 10. Component force as a percentage of freestream

Looking at the change in the static pressure distribution, figures 11 & 23, it is clear that the areas of most extreme low pressure are the most significantly affected; namely the front wing centerline, underfloor splitter (ΔC_P = +0.8) and rear wing mainplane suction surface (ΔC_P = +1.0). The rear wing mainplane and flap pressure surfaces also lose a nearly uniform pressure between ΔC_P = 0.7 and 0.8. The loss of the underfloor suction peak would explain the rearwards COP shift despite the rear wing losing the most downforce. Pressure on the majority of the floor behind the splitter increases by ΔC_P = +0.1 to +0.2, with a higher magnitude change of ΔC_P = +0.3 on the centerline.

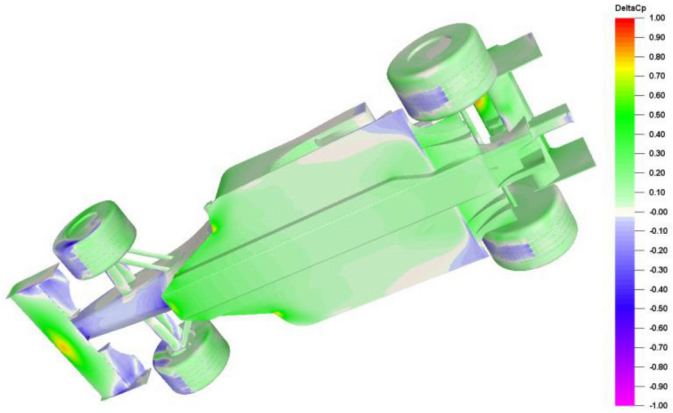

Figure 11. Surface ΔC_P for full wake case

Behind the car the effect of the inlet wake is that the magnitude of the upwash, figure 12, is reduced. The 'y' component of the 'lead car' wake is also still present up to and beyond the rear wing of the car. Meanwhile the centerline profile of the axial velocity, figures 4 & 18, has a similar profile to that of the freestream wake, but with increased velocity deficit, continuing further behind the car.

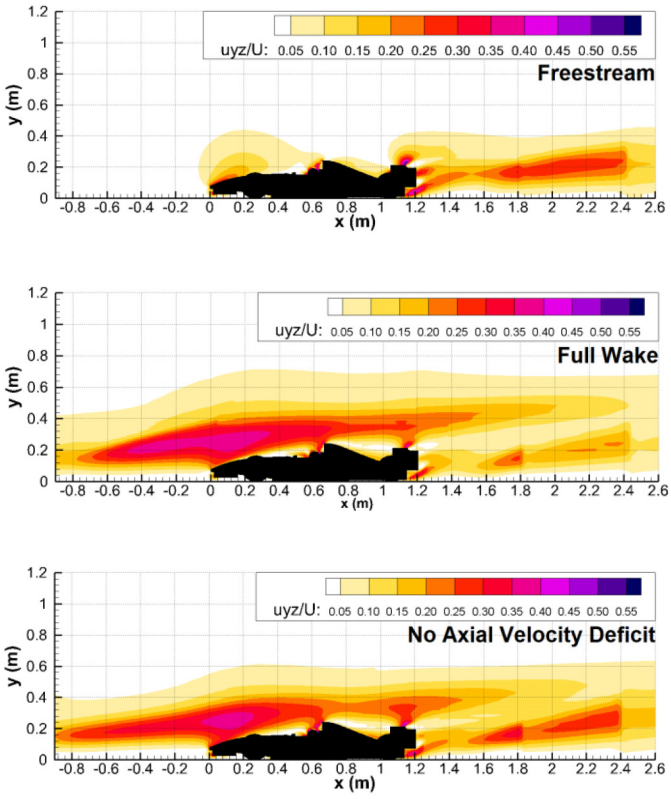

Figure 12. Centerline secondary velocity contours

No Axial Velocity Deficit

A formula car is a relatively bluff shape, especially the wheels and rear wing; consequently the wake features a large axial velocity deficit. Other flow features, such as the vorticity, will reduce the axial momentum in the wake, as shown by figure 19 whereby beyond 0.5 L_C downstream of the car the highest deficit is found in the vortex cores. The removal of axial velocity deficit in the very near wake (<0.25 L_C) would therefore be more associated with a decrease of the upstream body drag or reduced C_DA than a reduction of downforce.

The axial velocity was mostly removed from the inlet (which can be seen in figure 24), though with a small deficit (<4% u_∞) resulting from the secondary flows which are recreated at the inlet. The main static and stagnation pressure are consistent with the desired specifications, P_∞ and PO_∞. Although the profiles where the pressures deviate from freestream are not perfectly recreated, the removal of axial velocity has had a greater effect on the stagnation pressure than expected, even with the appropriate dynamic pressure added to the inlet. The shape of the static pressure contour is consistent with the full wake case, but with a $\Delta C_P = +0.2$ difference.

The result of the "no velocity deficit" wake is a recovery of the component forces towards the freestream, figure 10. The front wing even produces 5% more downforce, though the efficiency is lower due to 27% greater drag than the freestream case. While front wing downforce increases relative to freestream and the underfloor and rear wing loose performance the center of pressure shifts rearward by 6.7% of the wheelbase, figure 8. This can be attributed to a combination of the loss of the peak suction at the leading edge of the floor and a relative increase in front wheel and bodywork lift over the full wake case.

The surface static pressure delta, figures 13 & 25, shows that the pressure differences resulting from the inlet wake are minimal. The front wing suction pressure is reduced from the freestream case by $\Delta C_P = -0.1$, although as the static pressure at the inlet at front wing height is $\Delta C_P = -0.3$ this may be a result of the pressure rather than removal of the velocity deficit. The leading edge suction pressure peak is unaffected by the wake, however there is a small suction pressure loss at the mid-floor and diffuser.

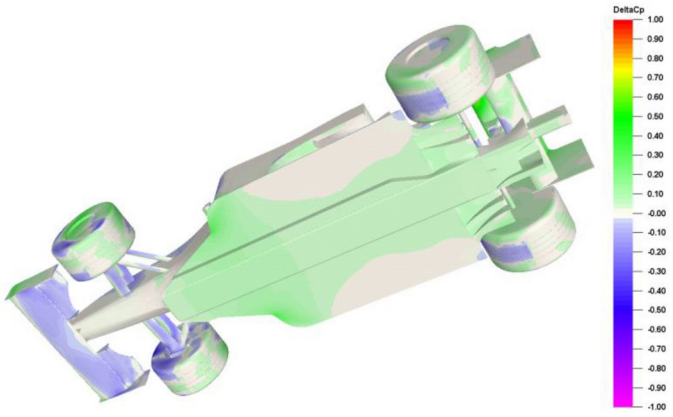

Figure 13. Surface ΔC_P for no axial velocity case

Centerline secondary flows (figure 12) over the front of the car are of lower magnitude than the full wake, but like the full wake the flow accelerating over the nose increases the velocity compared to the sampled wake. Like the full wake case the upwash in the wake is present over the whole car to the rear wing.

Sensitivity to Secondary Flows

The easiest variable to manipulate, due to its low impact on dynamic pressure, is the secondary velocity. As u_Y and u_Z each peak at about 22% of freestream velocity, the effect of $q_{Y,Z}$ on P_O is very small, see equation 1. In the very near wake ($\ll$0.25 L_C behind the car) secondary flows emanating from the wheels and diffuser make for a complex wake with a number of co and counter rotating vortices. By 0.25 L_C aft of the car the vortices merge with the dominant rear wing counter-rotating vortex pair, which is energized by a strong upwash from the rear diffuser. This vortex pair is a significant component of the wake and will become stronger as downforce increases, making secondary flow sensitivity the most practicable wake variable for study.

No Secondary Flows

Using a design of experiments type approach, the first case run is the "no secondary flows" case. This case approximates the wake of a car generating its downforce in a pure ground effect ideal. To produce the same level of downforce a wing out of ground effect will have to be inclined at a greater angle of attack than a wing in ground effect, thus the incidence of the wake is lower [13]. It should be noted that there would inevitably be some vorticity in the wake of a ground effect vehicle which is not simulated, but this vorticity would be weaker and lower than that emanating from the rear wing.

Like the "no axial velocity deficit" case the secondary flows on the inlet are almost uniform, but there is a residual <1% u_∞ secondary flow which appears to be caused by the boundary between two velocity levels, though this is random in nature, decays rapidly and does not form a vortex pair. Axial velocity and stagnation pressure deficits are recreated to the correct contour level, though the static pressure profile is uncontrolled, meaning the high P_O deficit vortex cores form the sampled wake are missing.

The efficiency of the downforce producing components is almost identical to the full wake case, though the actual drag and downforce levels are significantly reduced. The front wing drops to about 24% of the freestream downforce, while underfloor and rear wing are ~27-30% freestream. As well as the downforce producing components front wheel and bodywork lifts are also reduced, to 5% and 24% of freestream respectively (figure 17). Looking at the overall vehicle forces, figure 14; drag drops to 59% of the freestream, whereas the full wake case is 74%. This is not unexpected as the upwash in the wake will push the wake over the trailing vehicle to some extent. What is surprising is that downforce is only 0.4% lower than the full wake case, especially considering the front & rear wings and underfloor produce 30-50% of the downforce of the full wake, but this is explained by less lift from wheels and bodywork, as described earlier.

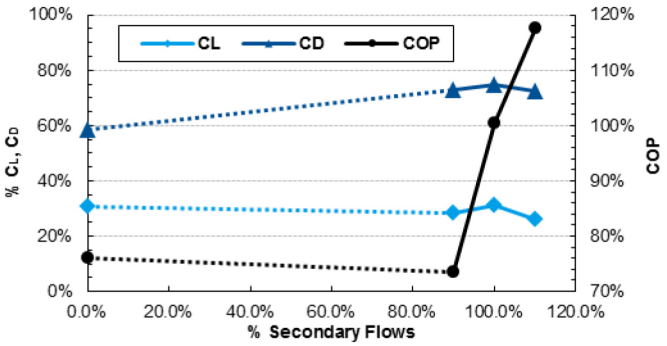

Figure 14. Vehicle drag, downforce as a percentage of freestream and absolute COP vs percentage secondary flows

Like the full wake case the no secondary flows case results in the COP migrating rearwards, but in this case only by 12%. From the surface pressure ΔC_P (figures 15 and 27) it is clear that the front wing suction pressure is almost totally eliminated with a greater than ΔC_P = +1.0 pressure increase over almost the whole mainplane, rather than just the centerline like the full wake case. The underfloor splitter and centerline pressure loss is similar to the full wake case though the mid-floor is almost unchanged from the freestream; the diffuser pressure is almost uniformly increased by ΔC_P = +0.3 relative to the full wake case, contributing to the significant downforce loss relative to the full wake case.

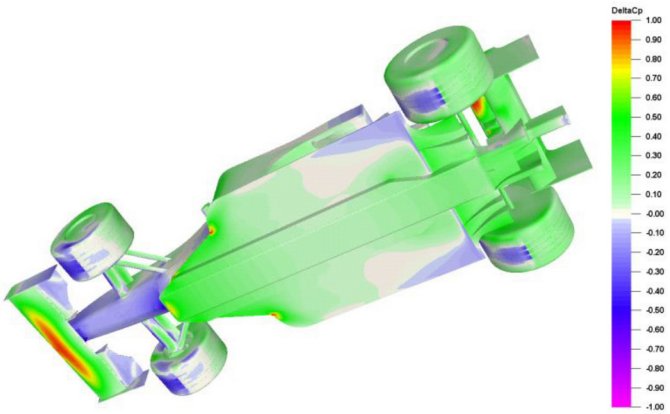

Figure 15. Surface ΔC_P for no secondary flows case

As well static pressure in the low pressure regions increasing, the high pressure regions such as the front and rear wing pressure surfaces are significantly affected (ΔC_P = −0.6 to −0.75). The stagnation points on the nose and floor leading are totally removed, ΔC_P = −1.0. The key, as shown in figure 16, is that the downstream vehicle is within a tunnel of low velocity. While secondary flows might locally have a detrimental impact on the following vehicle, overall they have the important impact of moving the wake up over following vehicles. This applies in particular to upwash.

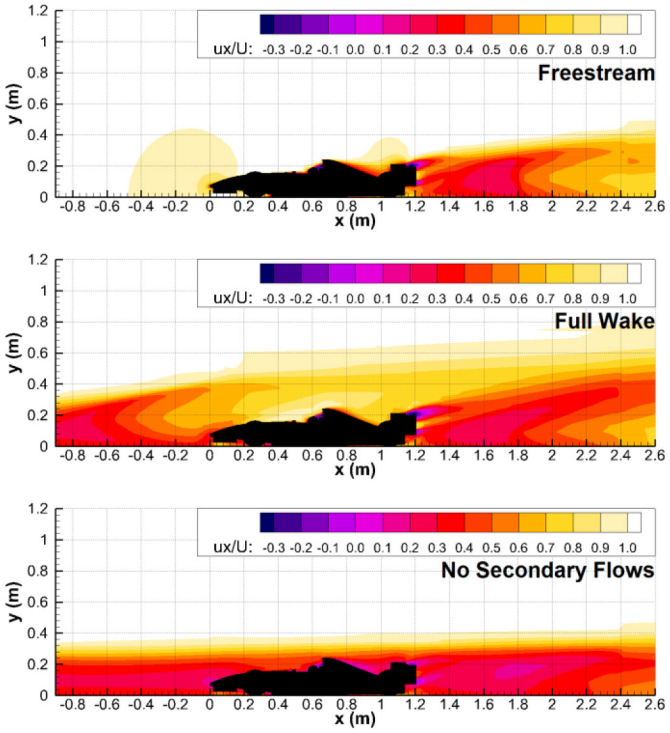

Figure 16. Centerline axial velocity contours

±10% Secondary Flows

The inlet for the 90% and 110% secondary flows cases more closely resemble the full wake (100% secondary flows case) than the no secondary flows case. The 90% $u_{Y,Z}$ case simulates a reduction of downforce of the upstream vehicle, mainly resulting from reduced rear wing aerodynamic performance. The 110% case would be a result of increased rear wing performance. The effect of the change on the inlet compared to the full wake is almost negligible, being only ±2.2% of u_∞. The change of u_Y and u_Z does not change the incident angle of the wake compared to the full wake, figures 12 & 16. Instead the effect is a small local change of $u_{Y,Z}$ intensity between the inlet and nose, with a small local change of incidence.

Vehicle drag resulting from the lower secondary flows on the inlet seems to be linear between the 0% and full wake cases, figure 14. Downforce for the whole vehicle however is non-linear and is 28% of freestream, albeit only 3% lower than the full wake case. Front and rear wing efficiencies are almost identical to the full wake case; though underfloor efficiency is slightly lower than −14. Downforce and drag from the wings and underfloor are slightly below the full wake as well. The COP shifts rearwards, as with all the wake cases, but only 10% rather than 37% for the full wake.

The vehicle downforce for the higher secondary flows case is the lowest of the secondary flows sensitivity cases, figure 14, and is only ~26% of freestream. Vehicle drag also reaches a plateau at 100% $u_{Y,Z}$ but is only 3% lower for this case. The downforce producing component efficiencies are similar to the full wake, with only the underfloor at a lower efficiency, but not as low as the 90% secondary flows case. All the component forces are 1-2% closer to freestream than the 90% case. The lifting bodies, especially front wheels and upper body are 8% and 4% closer to the freestream respectively

(figure 17). As mentioned earlier the front wheels generate a large lift which would contribute to the 17% further rearward COP than the full wake case. Another contributing factor is that the combined body and underfloor force is a resultant lift in these cases, with the body lift exceeding the underfloor downforce (figure 17).

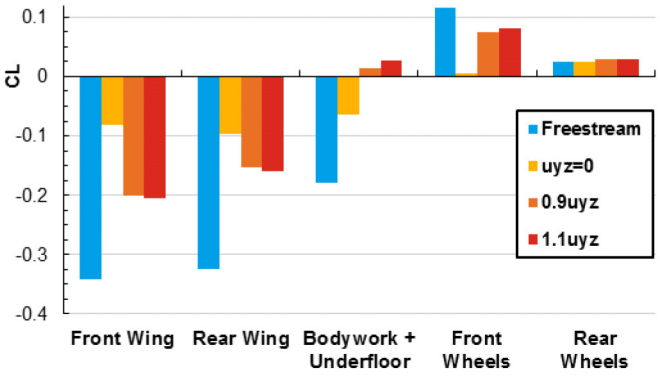

Figure 17. Component C_L for secondary flows sensitivity cases

Increasing secondary flow around a realistic value moved COP progressively rearwards (illustrated in figure 14). As discussed previously, the "no secondary flows" case is completely different from cases with realistic levels of secondary flow. The 54% rearwards shift of the COP for the $1.1u_{YZ}$ case (compared with free stream) puts it behind the rear wheel centerline and would result in a significant increase of understeer and a very uncomfortable and possibly dangerous experience for the driver. Dominy [1] and Howell [2] discuss similar extreme rearwards shifts in center of pressure for following vehicles.

For both cases, surface pressure (figures 18, 28 & 29) is almost identical to the full wake. Both cases see a marginally greater pressure difference on the underside centerline of the front wing, with the 90% case being a higher magnitude. In the 90% case the rear underfloor and diffuser is ΔC_P = ~0.05 higher than the full wake, while in the 110% case it is the front of the floor which is ΔC_P = +0.1 higher.

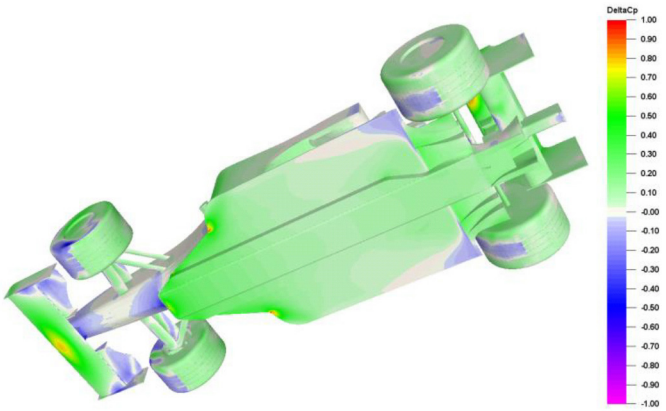

Figure 18. Surface ΔC_P for 110% secondary flows case

The non-monotonic impact of varying secondary flow intensity (eg: figure 14) reinforces the point that the impacts of secondary flow include both positive aspects (moving the wake over the following vehicle) and negative aspects (local off-design flow incidence on the following vehicle).

CONCLUSIONS

- The technique of setting the CFD inlet to match a sampled car wake provides a useful approach with good correlation on overall vehicle performance compared with a multi-vehicle simulation. Important differences remain for component forces, suggesting the importance of the upstream vehicle wake unsteadiness which is omitted when a time-averaged wake is used.
- Setting the wake using CFD allows the wake parameters to be varied directly. This allows ground effect and out of ground effect geometry sensitivity to wake components to be independently evaluated from car design. It should be noted that there are some challenges in the implementation due to the interaction between parameters.
- The upwash in the wake appears to be an important factor in pushing the wake over a following vehicle which reduces loss. Removing the upwash from the wake has the most negative effect on the trailing vehicle, upwash is not simple to decouple from secondary flows.
- Changing u_Y and u_Z by ±10% does not result in amonotonic impact on drag and downforce, illustrating the complexity of the many interactions of elements of the wake with the downforce producing elements on the following vehicle.
- It should be noted that the surfaces of a fully optimized Formula car could be closer to stall and could therefore be more susceptible to variations in upstream flow conditions.

REFERENCES

1. Dominy, R., *The influence of slipstreaming on the performance of a Grand Prix racing car.* Proceedings of the Institution of Mechanical Engineers, Part D: Journal of Automobile Engineering, 1990. 204(1): p. 35-40.
2. Howell, J., *Catastrophic lift forces on racing cars.* Journal of Wind Engineering and Industrial Aerodynamics, 1981. 9(1): p. 145-154.
3. Newbon, J.J. *Investigation into the effect of the wake from a generic formula one car on a downstream vehicle*. In *Institution of Mechanical Engineers International Vehicle Aerodynamics Conference*. 2014. Loughbrough.
4. Watts, M. and Watkins, S., "Aerodynamic Structure and Development of Formula 1 Racing Car Wakes," SAE Int. J. Passeng. Cars - Mech. Syst. 7(3):1096-1105, 2014, doi:10.4271/2014-01-0600.
5. FIA *2014 FIA Formula One Technical Regulations*. 2014.
6. Wilson, M., Dominy, R., and Straker, A., "The Aerodynamic Characteristics of a Race Car Wing Operating in a Wake," *SAE Int. J. Passeng. Cars - Mech. Syst.* 1(1):552-559, 2009, doi:10.4271/2008-01-0658.
7. Zhang, X., Toet W., and Zerihan J., *Ground effect aerodynamics of race cars.* Applied Mechanics Reviews, 2006. 59(1): p. 33-49.
8. Zerihan, J. and Zhang X., *Aerodynamics of a single element wing in ground effect.* Journal of Aircraft, 2000. 37(6): p. 1058-1064.
9. Zhang, X. and Zerihan J., *Aerodynamics of a double-element wing in ground effect.* AIAA journal, 2003. 41(6): p. 1007-1016.
10. Ahmed, M.R. and Sharma S., *An investigation on theaerodynamics of a symmetrical airfoil in ground effect.* Experimental Thermal and Fluid Science, 2005. 29(6):p.633-647.
11. Zhang, X., et al. *Tip vortices generated by a wing in ground effect*. in *Proceedings of the 11th International Symposium on Applications of Laser Techniques to Fluid Mechanics*. 2002. Citeseer.
12. Zhang, X. and Zerihan J., *Edge vortices of a double element wing in ground effect.* Journal of aircraft, 2004. 41(5): p. 1127-1137.
13. Zhang, X. and Zerihan J., *Turbulent wake behind a single element wing in ground effect.* transition, 2002. 1(1.5): p. 1.6.

14. Soso, M. and Wilson P., *Aerodynamics of a wing in ground effect in generic racing car wake flows.* Proceedings of the Institution of Mechanical Engineers, Part D: Journal of Automobile Engineering, 2006. 220(1): p. 1-13.
15. Soso, M. and Wilson P., *The influence of an upstream diffuser on a downstream wing in ground effect.* Proceedings of the Institution of Mechanical Engineers, Part D: Journal of Automobile Engineering, 2008. 222(4): p. 551-563.
16. Soso, M.D., *Wings In Ground Effect*. 2002, University of Illinois.
17. Straker, A., *The influence of slipstreaming on racing car wing performance*. 2007, Durham University.
18. Swalwell, K.E., *The effect of turbulence on stall of horizontal axis wind turbines*. 2005, Monash University.
19. Mankowski, O., *The Wind Tunnel Simulation and Effect of Turbulent Air flow on Automotive Aerodynamics*. 2013, Durham University.
20. Mankowski, O., Sims-Williams, D., and Dominy, R., "A Wind Tunnel Simulation Facility for On-Road Transients," *SAE Int. J. Passeng. Cars - Mech. Syst.* 7(3):1087-1095, 2014, doi:10.4271/2014-01-0587.
21. Schröck, D., Widdecke N., and Wiedemann J.. *Aerodynamic response of a vehicle model to turbulent wind*. in *7th FKFS Conference*. 2009.
22. Cogotti, A., "Update on the Pininfarina "Turbulence Generation System." and its effects on the Car Aerodynamics and Aeroacoustics," SAE Technical Paper 2004-01-0807, 2004, doi:10.4271/2004-01-0807.
23. Watkins, S. and Vino G., *The effect of vehicle spacing on the aerodynamics of a representative car shape.* Journal of wind engineering and industrial aerodynamics, 2008. 96(6): p. 1232-1239.
24. Vino, G., Watkins S., and Mousley P., *The passenger vehicle wake under the influence of upstream turbulence.* Fuel, 2003. 2011: p. 08-21.
25. Gaylard, A., Beckett, M., Gargoloff, J., and Duncan, B., "CFD-based Modelling of Flow Conditions Capable of Inducing Hood Flutter," *SAE Int. J. Passeng. Cars - Mech. Syst.* 3(1):675-694, 2010, doi:10.4271/2010-01-1011.
26. Newnham, P., *The influence of turbulence on the aerodynamic optimisation of bluff body road vehicles*. 2007, Loughborough University.
27. Mankowski, O., Sims-Williams, D., Dominy, R., Duncan, B. et al.,"The Bandwidth of Transient Yaw Effects on Vehicle Aerodynamics," *SAE Int. J. Passeng. Cars - Mech. Syst.* 4(1):131-142, 2011, doi:10.4271/2011-01-0160.
28. Kandasamy, S., Duncan, B., Gau, H., Maroy, F. et al.,"Aerodynamic Performance Assessment of BMW Validation Models using Computational Fluid Dynamics," SAE Technical Paper 2012-01-0297, 2012, doi:10.4271/2012-01-0297.
29. Sprot, A., *Open-wheel aerodynamics: effects of tyre deformation and internal flow*. 2013, Durham University.

CONTACT INFORMATION

Joshua J. Newbon
joshua.newbon@durham.ac.uk

David B. Sims Williams
d.b.sims-williams@durham.ac.uk

Robert G. Dominy
robert.dominy@northumbria.ac.uk

ACKNOWLEDGMENTS

The authors are grateful to Jaguar Land Rover and the EXA Corporation for the use of the PowerFLOW software suite. Joshua Newbon is funded by the Engineering and Physical Sciences Research Council (EPSRC).

DEFINITIONS/ABBREVIATIONS

COP - Center of pressure

μ - Dynamic viscosity

ρ - Fluid density

C_D - Drag coefficient

C_L - Lift coefficient

C_P - Static pressure coefficient

C_{PO} - Stagnation (total) pressure coefficient

D - Aerodynamic drag

I_X - Axial turbulence intensity

L - Aerodynamic lift

L/D - Aerodynamic efficiency

L_C - Characteristic length

P - Static pressure

P_O - Stagnation pressure

q - Dynamic pressure

Re - Reynolds number, $\rho u L_C/\mu$

u_X - x-axis aligned velocity

u_Y - y-axis aligned velocity

u_Z - z-axis aligned velo

$u_{Y,Z}$ - Secondary flows, $\sqrt{u_Y^2 + u_Z^2}$

∞ - Freestream

APPENDIX

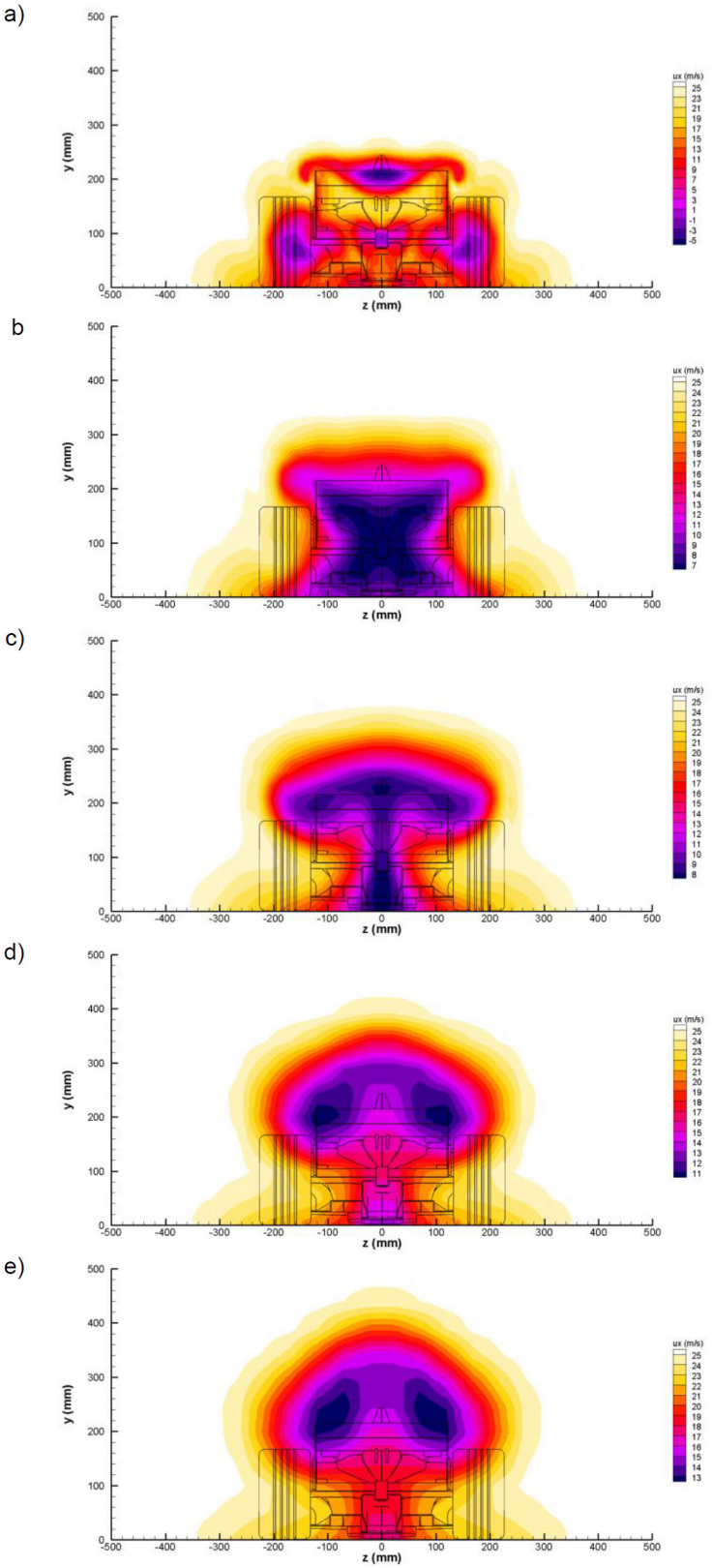

Figure 19. Freestream wake development, axial velocity (top to bottom $0L_C$, $0.25L_C$, $0.5L_C$, $0.75L_C$ & L_C)

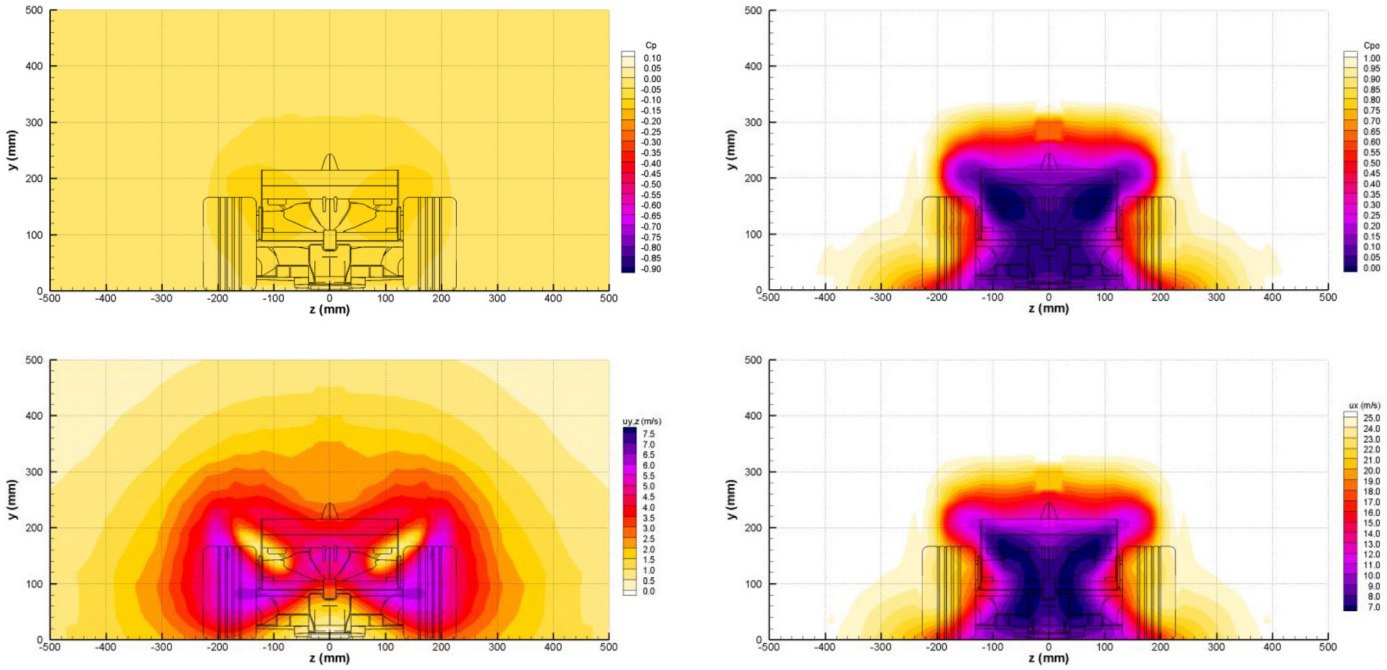

Figure 20. Sampled wake contours (clockwise from top left C_P, C_{PO}, u_X and $u_{Y,Z}$)

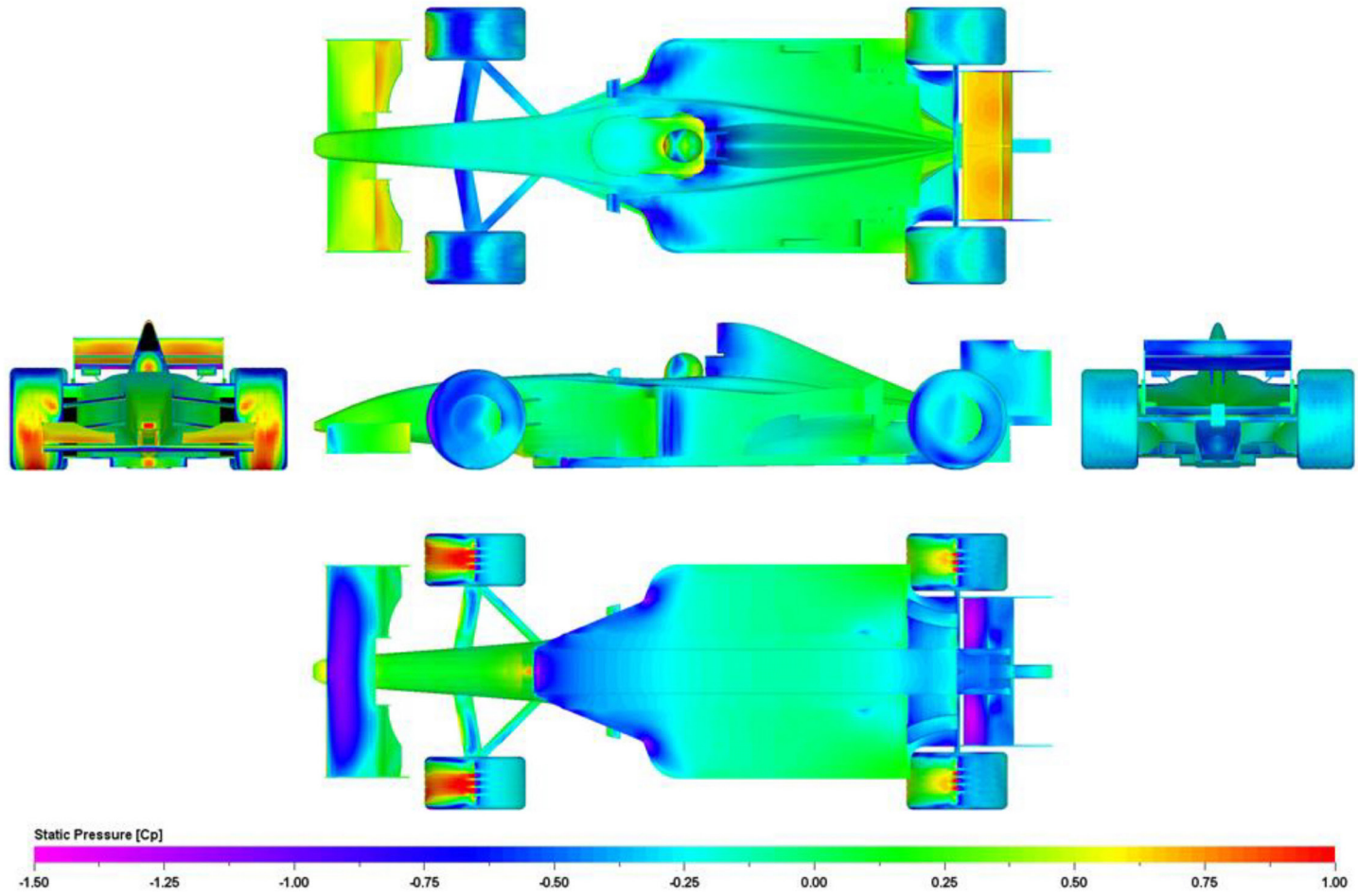

Figure 21. Freestream surface static pressure distribution

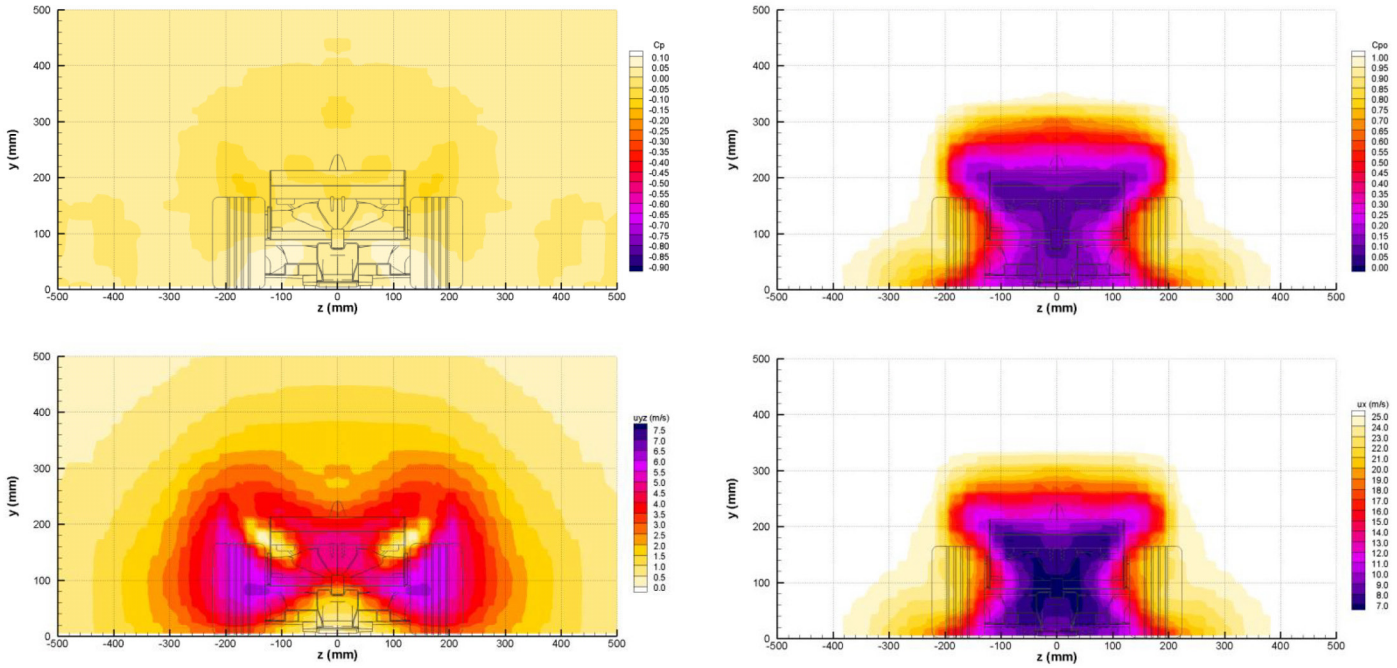

Figure 22. Inlet contours for full wake case (clockwise from top left C_P, C_{PO}, u_X and $u_{Y,Z}$)

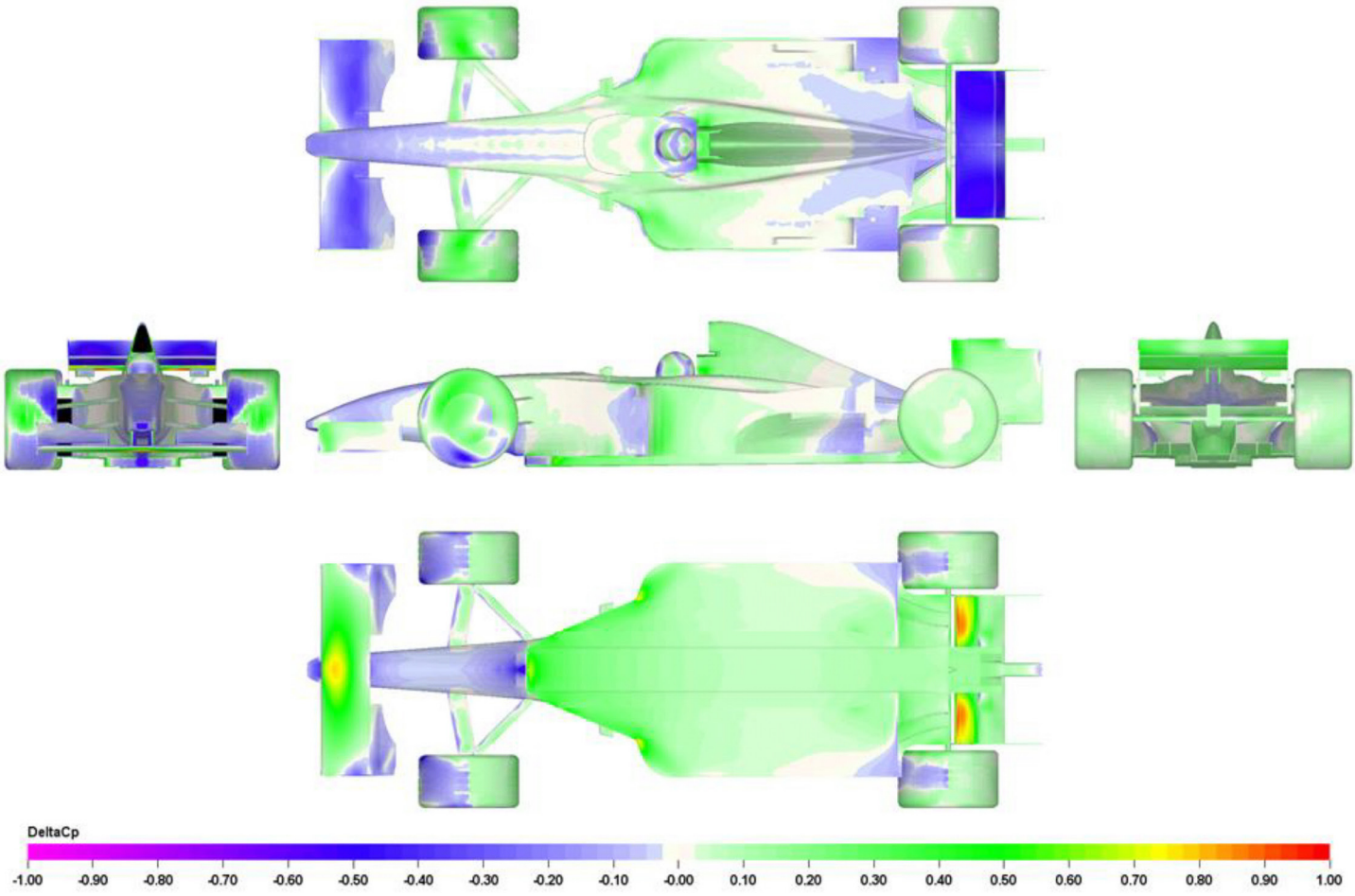

Figure 23. Surface ΔC_P for full wake case

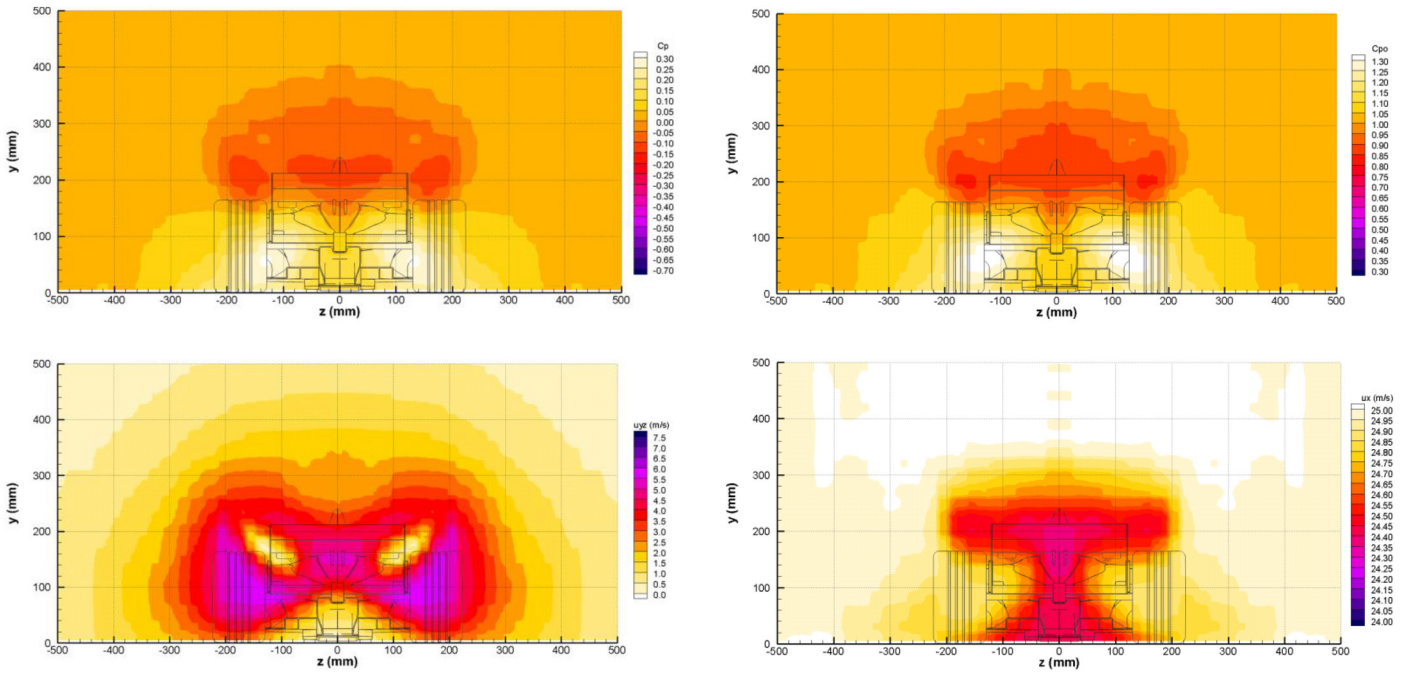

Figure 24. Inlet contours for no axial velocity deficit case (clockwise from top left C_P, C_{PO}, u_X and $u_{Y,Z}$)

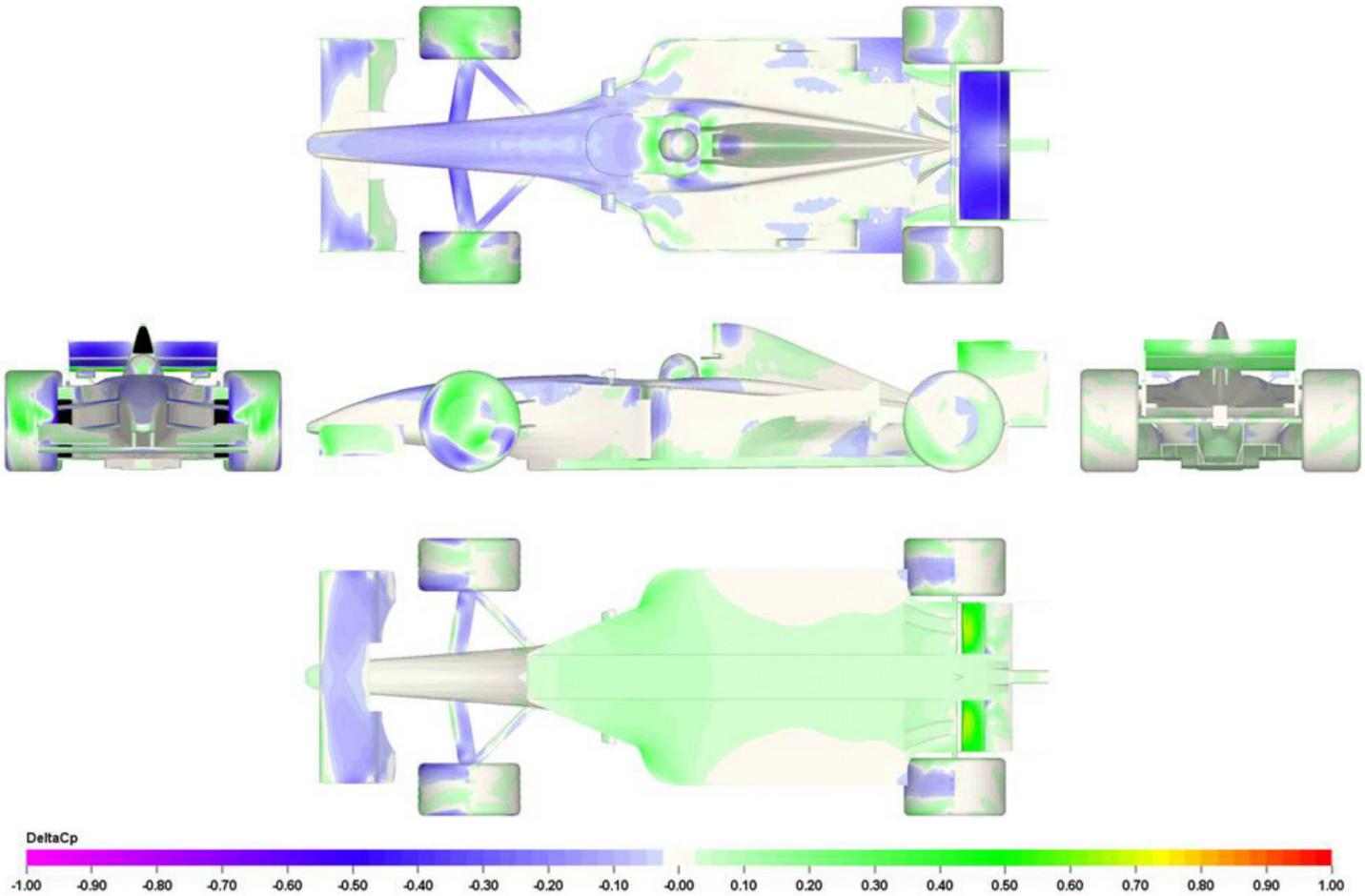

Figure 25. Surface ΔC_p for no axial velocity deficit case

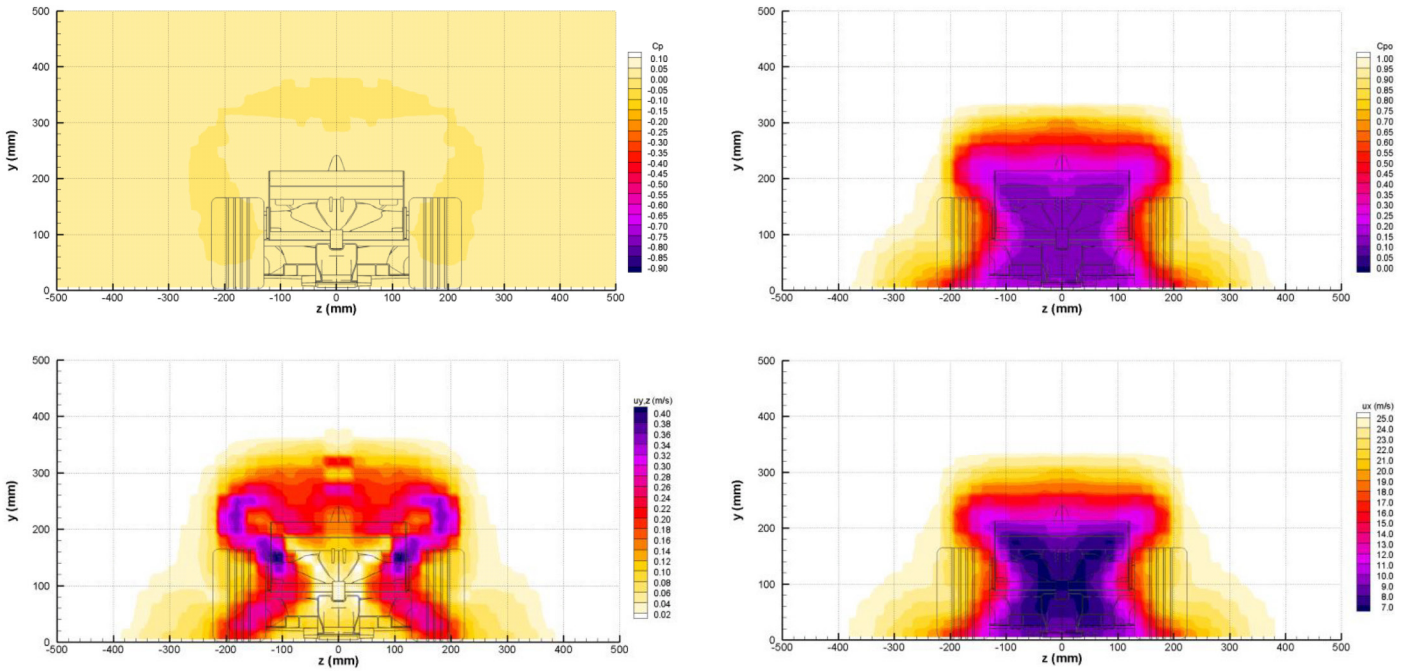

Figure 26. Inlet contours for no secondary flows case (clockwise from top left C_P, C_{PO}, u_X and $u_{Y,Z}$)

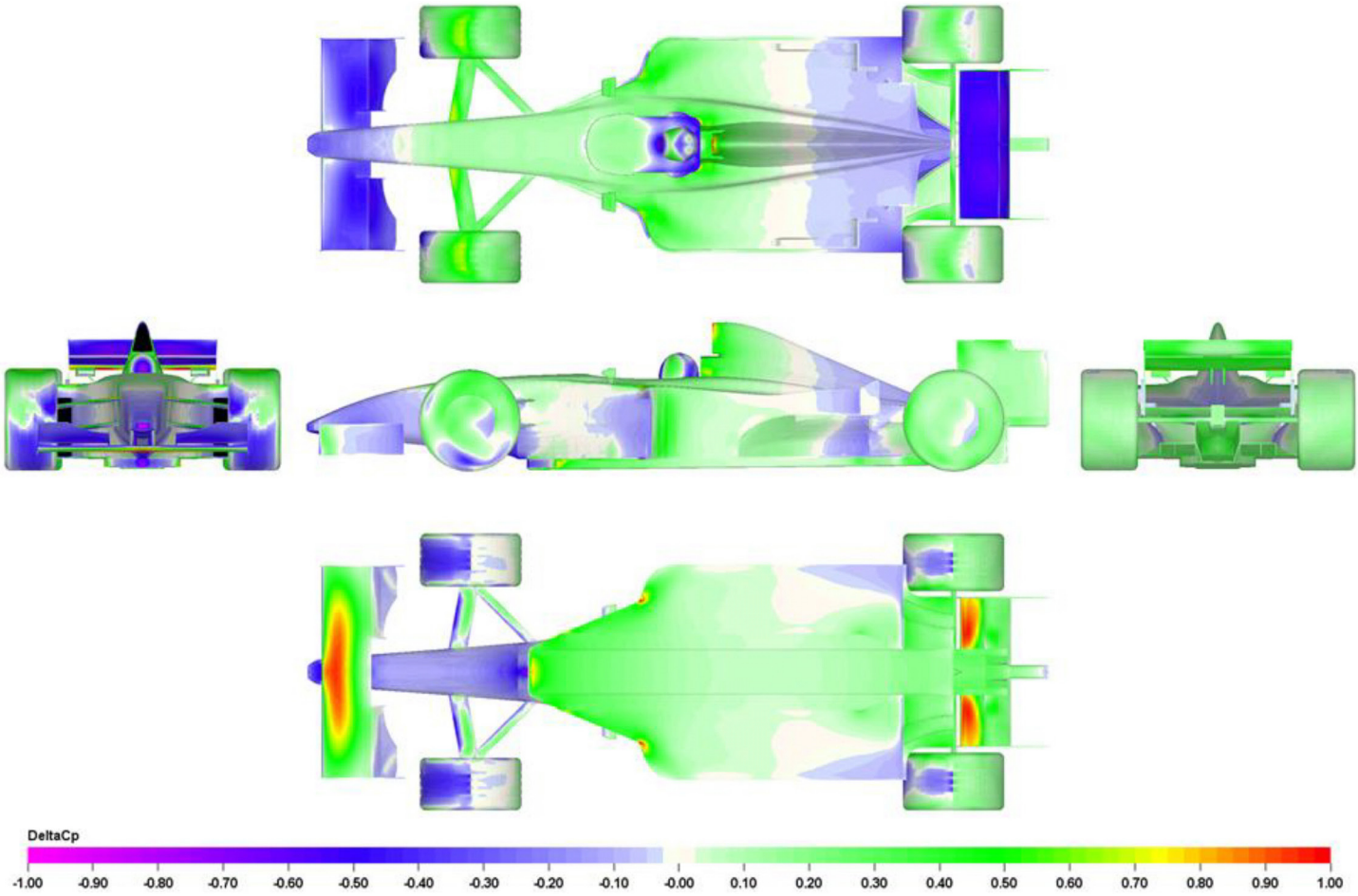

Figure 27. Surface ΔC_p for no secondary flows case

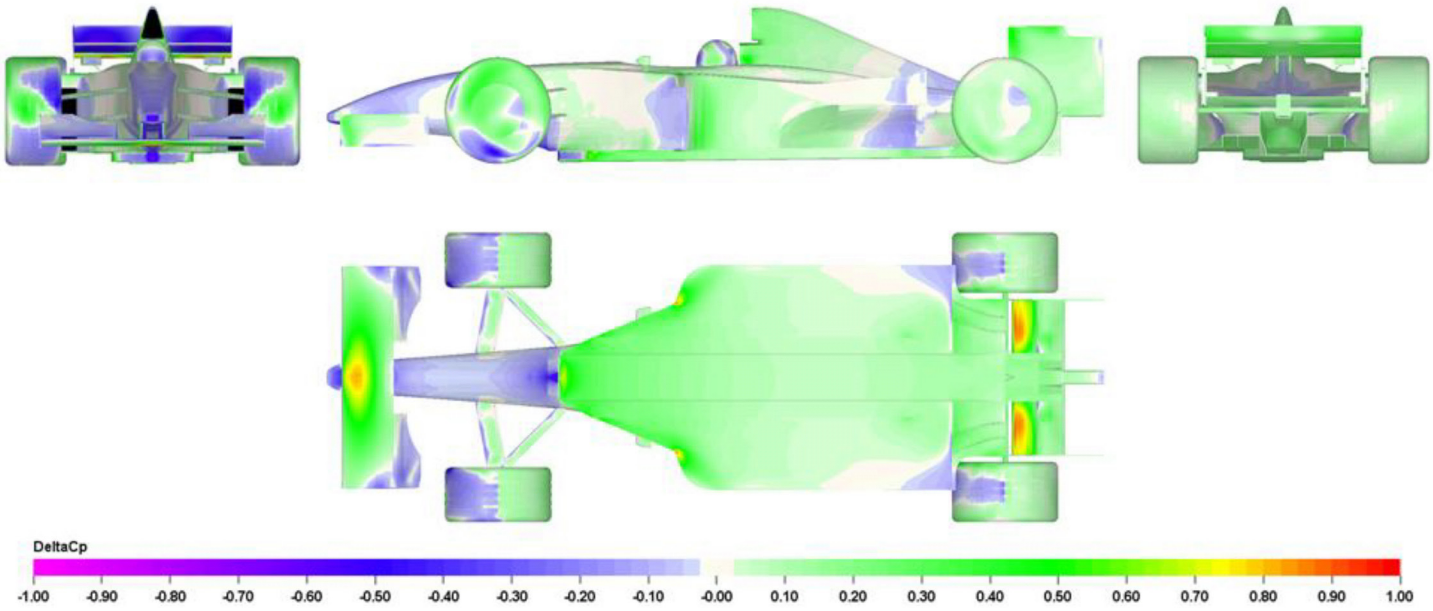

Figure 28. Surface ΔC_p for 90% secondary flows case

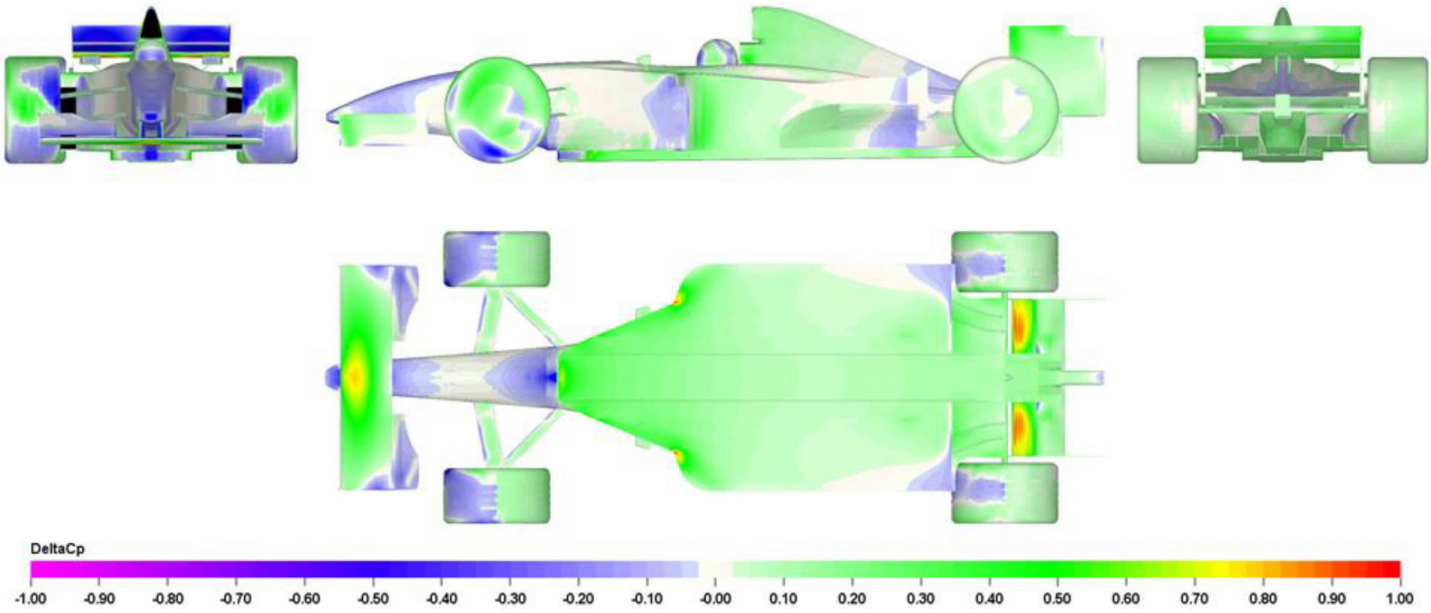

Figure 29. Surface ΔC_p for 110% secondary flows case